Sensors and Materials, Vol. 25, No. 8 (2013) 567–576
MYU Tokyo

S & M 0949

pH Response of Silicon Nanowire Sensors: Impact of Nanowire Width and Gate Oxide

Kristine Bedner*, Vitaliy Anatolijovic Guzenko, Alexey Tarasov[1], Mathias Wipf[1], Ralph Lukas Stoop[1], David Just[1], Sara Rigante[2], Wangyang Fu[1], Renato Amaral Minamisawa, Christian David, Michel Calame[1], Jens Gobrecht and Christian Schönenberger[1]

Laboratory for Micro- and Nanotechnology, Paul Scherrer Institute, PSI Villigen, Switzerland
[1]Department of Physics, University of Basel, Basel, Switzerland
[2]École Polytechnique Fédéral de Lausanne, Lausanne, Switzerland

(Received January 9, 2013; accepted May 9, 2013)

Key words: pH response, nanowire sensor, gate oxide, ion-sensitive field-effect transistor

We present a systematic study of the performance of silicon nanowires (SiNWs) with different widths when they are used as ion-sensitive field-effect transistors (ISFETs) in pH-sensing experiments. The SiNW widths ranged from 100 nm to 1 μm. The SiNW-ISFETs were successfully fabricated from silicon-on-insulator (SOI) wafers with Al_2O_3 or HfO_2 as gate dielectric. All the SiNWs showed a pH Response close to the Nernstian limit of 59.5 mV/pH at 300 K, independent of their width, or the investigated gate dielectric or operating mode. Even nanowires (NWs) in the 100 nm range operated reliably without degradation of their functionality. This result is of importance for a broad research field using SiNW sensors as a candidate for future applications.

1. Introduction

In recent years, the ion-sensitive field-effect transistor (ISFET)[1,2] has been scaled down to a silicon nanowire ISFET (SiNW-ISFET) with sub-100 dimensions.[3–6] The reduced size offers unique possibilities, such as the dense integration of multiplexed NWs,[7,8] which sense a large number of different target molecules simultaneously using differently functionalized NWs.[9] The key feature for biological applications is that nanostructures are on the scale of biological specimens. Recently, Tian *et al.*[10] have demonstrated a manipulation of the living cell with nano-FETs without damaging the cell.

*Corresponding author: e-mail: Kristine.Bedner@psi.ch

The sensing mechanism of SiNW-ISFETs is based on the accumulation of charged molecules on the NW surface, which leads to a surface potential shift. The transistor then responds to changes in the surface potential with a threshold voltage shift ΔV_{th}. In a pH-sensing experiment, the accumulated surface charge originates from OH groups located on the surface of the gate dielectric, which are positively (protonated) or negatively (deprotonated) charged, according to the pH of the buffer solution. This surface charge provokes the pH response of the SiNW-ISFET in the form of a threshold voltage shift. Consequently, the pH response is given in mV/pH. Several publications addressed the question on whether the NW width(4,11–13) or thickness(14,15) has an effect on the pH response; however, the results were inconsistent. An effect of the NW width on the response in pH-sensing experiments has been shown in refs. 12 and 13. Elfström *et al.*(12) observed an increasing threshold voltage shift with decreasing NW width. No pH response was found for NW widths > 150 nm. Vu *et al.*(4) reported preliminary results for single 80- and 400-nm-wide wires that exhibit the same threshold voltage shift of 41 mV/pH. Moreover, the ideal working point showing the highest pH response is also a controversial discussion in the literature. Gao *et al.*(16) demonstrated an enhancement of the pH response in the subthreshold regime compared with that in the linear regime, whereas preliminary results described in ref. 4 suggest the same pH response in both regimes. To clarify these disagreements, we explore in a systematic manner the effect of the NW width of SiNW-ISFETs on the pH response with widths ranging from 1 μm down to 100 nm in both operating modes, the subthreshold and linear modes. In addition, we study the sensing properties of the SiNW-ISFET coated with Al_2O_3 and HfO_2 grown by atomic layer deposition (ALD). Compared with SiO_2,(4,10,11,16) these oxides provide a leakage-free(17) operation with an ideal Nernstian pH response that is independent of the salt concentration.(5,6,18) For the application of wide pH ranges, HfO_2 is a predestined candidate as a sensing surface due to its chemical inertness in most acidic or basic solutions.

2. Materials and Methods

The SiNW-ISFETs were fabricated from silicon-on-insulator (SOI) wafers following the top-down approach.(11) The SOI wafer (Soitec, France) has a buried oxide layer of 145 nm and an 85-nm-thick low-doped p-Si(100) device layer with a resistivity of 8.5 to 11.5 Ω·cm. First, the Si device layer was thermally oxidized with a 15-nm-thick SiO_2 layer. Then, the pattern of the SiNW-ISFET was defined by electron beam lithography (EBL) in a negative resist (AZ nLOF 2000) and transferred to the SiO_2 layer by reactive ion etching. The patterned SiO_2 was used as an etching mask for the wet chemical etching of the Si device layer in tetra-methyl ammonium hydroxide (TMAH) with 10 vol.% isopropanol (IPA) at 45 °C. The wet chemical etching of the Si(100) layer is highly anisotropic with etch rates depending on the crystallographic orientation of the silicon.(19) The Si(111) planes are etched approximately 100 times slower(11) than the other planes, which results in a trapezoidal shape of the NW cross section. A key feature of our sensors is that a single SiNW-ISFET chip contains 48 NWs with eight top widths W_{top} [Fig. 1(a)] ranging from 1 μm down to 100 nm. The 48 NWs are arranged in four arrays with twelve NWs sharing the common drain contact. The length of the NWs

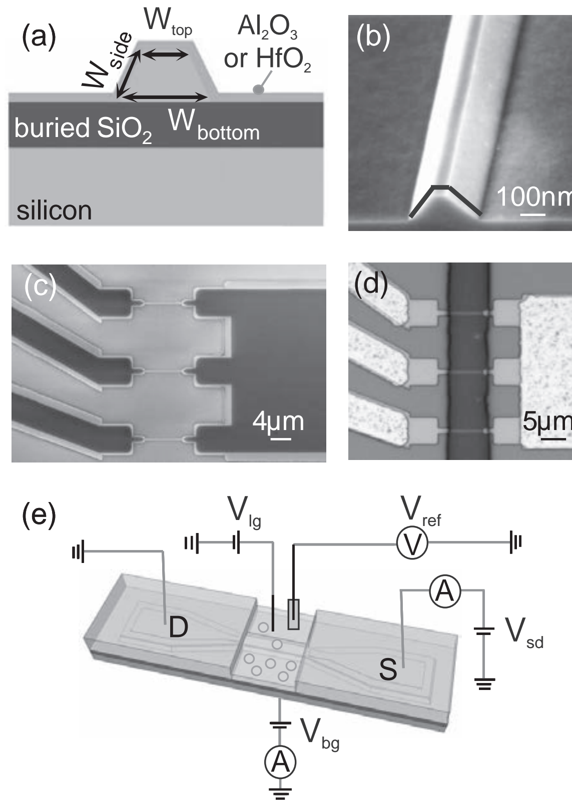

Fig. 1. (a) Schematic cross section of a wet-etched silicon NW fabricated from a (100) SOI wafer. It shows the top and bottom widths of the NW, W_{top} and W_{bottom}, respectively. The sidewalls W_{side} are formed by the Si(111) planes. As top oxide, Al_2O_3 or HfO_2 was used, grown by ALD. The thicknesses of the ALD oxides were 20 nm for Al_2O_3 and 10 or 20 nm for HfO_2. (b) Electron beam micrograph of a NW cross section. The solid blue line represents the effective wire width, $W_{eff} = W_{top} + 2W_{side}$. (c) Electron beam micrograph of a NW array showing three NWs (W_{top} = 100 nm) connected to the implanted (dark area) source contacts on the left and the common drain contact on the right. (d) Micrograph of a NW array with three NWs (W_{top} = 100 nm) connected to the implanted contacts, which are covered by metal. SU-8 resist is used to form the vertical liquid channels on top of the NW array. (e) Schematics of the liquid measurement setup. A source-drain current I_{sd} flows through the NW as the source-drain voltage V_{sd} is applied. The external voltages V_{bg} and V_{lg} can be applied to the back gate and liquid gate, respectively. The reference electrode determines the potential V_{ref} in the liquid.

is 6 μm and their height is about 85 nm. The bottom and sidewall widths are denoted as W_{bottom} and W_{side}, respectively [Fig. 1(a)]. The top perimeter of the NW comprising the sum of W_{top} and both sidewalls is represented by the effective wire width, W_{eff} [Fig. 1(b)]. After the silicon etching, the pattern of the source and drain contacts was defined

in the PMMA resist by EBL. The resist acted as an implantation mask for the following implantation with a BF_2^+ dopant dose of 2.3×10^{15} cm^{-2} at 33 keV. The implanted area approached the NW to a distance of ~200 nm. The NW retained its original low p-type doping concentration. After implantation, the dopants were activated in a thermal annealing step at 950 °C for 6 min in forming gas. The NW array with three NWs connected to the implanted source and common drain contact is shown in Fig. 1(c). The passivation of the SiNW-ISFET, which is necessary for measurements in liquids, was carried out by atomic layer deposition (ALD) of Al_2O_3 and HfO_2 (Savannah S100 Cambridge NanoTech). The ALD oxides were deposited directly on the NW surface. Immediately prior to the ALD oxide growth, a Radio Corporation of America (RCA) cleaning was done. During the RCA cleaning, the 15-nm-thick thermal SiO_2 was etched in buffered hydrofluoric acid (BHF). After the growth of the ALD oxides, the pattern of the source/drain contact windows was defined by optical lithography in the resist AZ nLOF 2000. The contact windows were then opened in BHF. The etch rate of Al_2O_3 is comparable to that of thermal SiO_2, whereas HfO_2 etches 14 times slower. Immediately after the etching, the opened contacts were metalized with Al-Si(1%) in a lift-off process. The formation of the ohmic contacts was completed in a thermal annealing process in forming gas at 450 °C. In the same step, the ALD oxides were also postannealed. It is known that the postannealing of the ALD oxides in forming gas has the effect of reducing the density of interface states D_{it} as they are passivated by hydrogen.[20] Also, the dielectric constants of the oxides are affected as the oxide structure changes from amorphous to (poly)-crystalline, depending on the annealing temperature. However, the ALD oxides have a large excess of O_2 as they are grown in an oxygen-rich environment. Therefore, there is the risk that during the postannealing, the excess O_2 diffuses to the Si where it leads to the growth of the interfacial SiO_2 layer[20,21] that already formed between the Si substrate and the ALD oxide during the ALD deposition.[20] The smaller dielectric constant of 3.9 for SiO_2 will reduce the total dielectric constant of the ALD layer. To integrate the fluidic system, microchannels were fabricated in the SU-8 resist by optical lithography. Figure 1(d) shows a micrograph of the SiNW-ISFET after this process step. One microchannel aligned perpendicular to the NWs can be seen. After the wire bonding, the contact pads including the wire bonds were sealed with epoxy. In the experiment, the microchannel was filled with an electrolyte, and the electrostatic potential of this electrolyte was mediated through the liquid to the NWs. This is known as liquid gating. The pH-sensing measurements were carried out in standard pH buffer solutions (Titrisol, Merck) with different pH values. In Fig. 1(e), a schematic of the measurement setup is shown.[17,22] The device was operated at a source-drain voltage V_{sd} of 0.1 V and the conductance G through the device was measured. The conductance was modulated by a top liquid gate voltage V_{lg} that was applied to a platinum wire immersed in the buffer solution. A calomel reference electrode was used to measure the effective potential V_{ref} in the buffer solution against ground. Additionally, a back gate voltage V_{bg} can be applied to the back side of the sample. The measurements were performed with buffer solutions with pH values ranging from 3 to 9 and from 3 to 10, for Al_2O_3 and HfO_2, respectively. For Al_2O_3 the highest pH was 9 as the Al_2O_3 is etched at higher pH values. The basic buffers did not attack the HfO_2 layer due to its chemical inertness to

acidic or basic solutions, apart from hydrofluoric (HF) acid-based solutions. We started with the buffer at pH 3 and exchanged sequentially the buffers with steps of $\Delta pH = 1$ until the buffer with the highest pH was reached. We then returned stepwise to pH 3. All the 48 NWs of one SiNW-ISFET chip were measured automatically at different pH values with a LabView-controlled measurement setup including a switching box (Keithley 3706).

3. Results and Discussion

Figure 2(a) shows the conductance G on a logarithmic scale as a function of reference voltage V_{ref} for NWs with W_{top} of 100 nm and 1 µm, measured at pHs 4, 6, and 8. The hysteresis in the transfer curves for the forward and backward voltage sweep of V_{ref} is small and maximum 5 mV. The transfer curves shift to more positive V_{ref} values if the pH is increased,[8] which is in agreement with the site-binding model.[2] Here, to determine the pH response, we do not extract the threshold voltage V_{th} according to

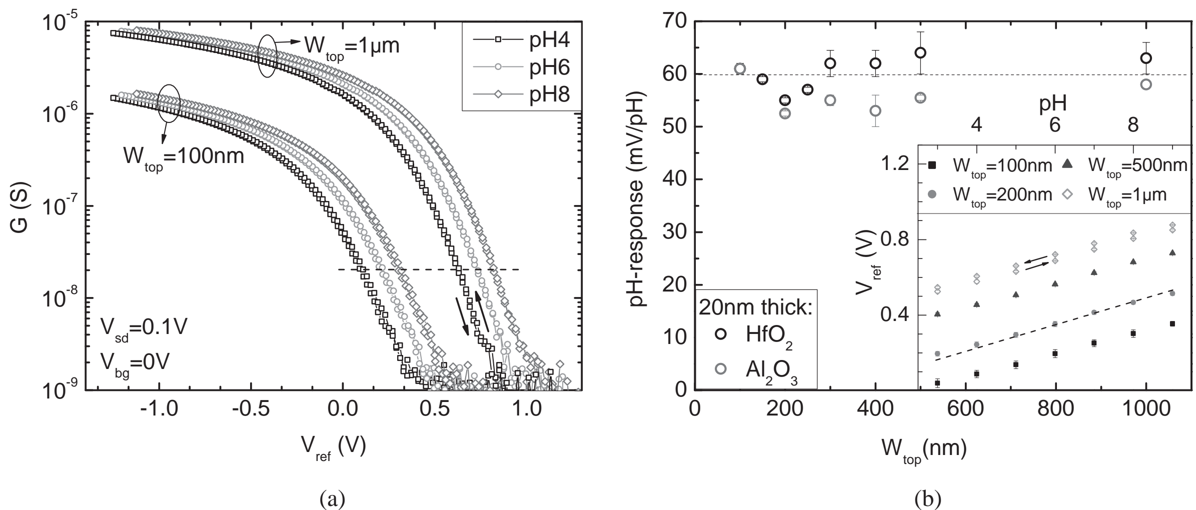

Fig. 2. (a) Logarithmic conductance G vs reference voltage V_{ref} for two NWs (W_{top} = 100 nm and 1 µm) measured at pHs 4, 6, and 8. Owing to the pH response, the transfer curves shift to the right with increasing pH. The transfer curves have a small hysteresis of maximum 5 mV in the forward and backward sweeps of V_{ref}. (b) The pH response of NWs with W_{top} ranging from 100 nm to 1 µm is close to the Nernst limit of 59.5 mV/pH at 300 K (black, dashed line). Buffer solutions with pH values from 3 to 9 for Al_2O_3 were used. An effect of the NW width or gate oxide on the pH response is not observed. Inset: The liquid potential V_{ref} extracted at 20 nS [Fig. 2(a) dashed line] is plotted as a function of pH. A linear dependence is found over the whole pH range. The pH response is defined by the slope of the best fit line. The NW with W_{top} = 1 µm shows the pH response for pH values measured from 3 to 9 and back to 3 with a negligible hysteresis.

one of the classical methods,[23] as we are not interested in the absolute V_{th} values. It is sufficient to know the relative shift of the transfer curves. Therefore, we defined V_{th} as the reference potential V_{ref} at any source-drain conductance value in the subthreshold regime. In our experiments, this value was 20 nS as indicated by the dashed line in the semilogarithmic plot of Fig. 2(a). Consequently, the threshold voltage shift ΔV_{th} was replaced by ΔV_{ref}. A set of V_{ref} values at 20 nS for different pH values are presented for four NW widths in the inset of Fig. 2(b). A linear dependence is found over the whole pH range. Moreover, a small negligible hysteresis in the forward and backward sweeps of the pH values is observed. (The drift rate of V_{ref} is a few mV/h for samples covered with 20-nm-thick Al_2O_3.) The slope of a linear fit to the data defines the pH response of the NW in mV/pH. These slopes are shown in Fig. 2(b) for NWs with W_{top} ranging from 100 nm to 1 µm. All the NWs show an ideal Nernstian behavior of 60 mV/pH at 300 K, independent of the NW width or gate oxide type and without degradation of the pH response over time. To the best of our knowledge, this is the first systematic study showing a clear absence of any size dependence on pH-sensing properties of NWs. The observed ideal pH response confirms recent results showing that ALD-grown Al_2O_3[18] and HfO_2[6] are excellent pH-sensing interfaces, owing to the high density of active surface groups that buffer the pH changes in the bulk solution. Within the site-binding model,[2] this oxide property is called the surface buffer capacity. As long as the oxide/electrolyte interface of the surface of the NW provides a large surface buffer capacity for protons, no size dependence is expected. Our observation is therefore in strong contrast to the work described in refs. 12 and 13.

In an application, it is convenient to measure a large conductance. For fast readout, it is therefore beneficial to operate the ISFETs in the linear regime and not in the subthreshold regime. In the linear regime, the measured signal is the conductance change ΔG (pH) at constant V_{ref}. It can be converted to a voltage shift ΔV_{ref} using the transconductance $g_m = dG/dV_{gate}$:

$$\Delta G(\mathrm{pH}) = g_m \Delta V_{ref}. \tag{1}$$

To investigate the influence of the NW width on the response of ΔG to pH changes in the linear regime, one has to carefully analyze the transconductance g_m. A comparison between different NW widths requires a normalization of the conductance because it changes with the wire size and shape.[24,25] Different methods could be assumed, such as normalization with the cross-sectional area of the wire, the top width W_{top}, the top perimeter $W_{eff} = W_{top} + 2W_{side}$, the bottom width W_{bottom}, or even the full perimeter of the wire $W_{eff} + W_{bottom}$. It is not clear a priori which method is the best, because we do not know the exact current distribution along the NW cross section. If the current flows homogeneously over the full cross section, one would have to scale with the area. There are many reasons, however, why this might not be the case. For example, we can gate the NW asymmetrically and thereby accumulate more carriers at the top surface as compared with the bottom surface, or vice versa. It is also known that surfaces with different crystallographic orientations have different band alignments;[21] hence, the accumulation of carriers may start differently at different crystal faces. Since a detailed systematic

study of these variabilities is beyond the scope of this work, we assume that the current scales with the top perimeter, i.e., $W_{eff} = W_{top} + 2W_{side}$. This assumption is motivated by the gating scheme via the liquid gate (top gate), which is used in the experiments in this work. It is further justified, because the electrolyte is in contact simultaneously with both the top and side faces. We thereby neglect the possible dependence of the current on the crystal orientation.

In Fig. 3(a), the transfer curves normalized by W_{eff} are shown for two NWs with W_{top} of 100 nm and 1 μm at different pH values. The linear regimes of both normalized transfer curves are very similar, which indicates an identical scaled transconductance for different wire widths. Moreover, the scaled transconductance values for a set of NWs with different W_{top} and HfO_2 or Al_2O_3 as gate oxide are shown in Fig. 2(b). The error bars result from an average over two NWs with an equivalent W_{top}. All the NWs with different widths show a similar scaled transconductance. On the basis of this result, we can conclude that in the linear regime, the normalized conductance change ΔG, and therefore, the response to pH changes, is also independent of the NW width and the operating regime. Our result is in contrast with the results shown by Gao *et al.*(16) Therefore, our results prove that one can fabricate NW sensors with ideal Nernstian behaviour with NWs down to 100 nm width, and an operation in the linear and subthreshold regimes is favourable.

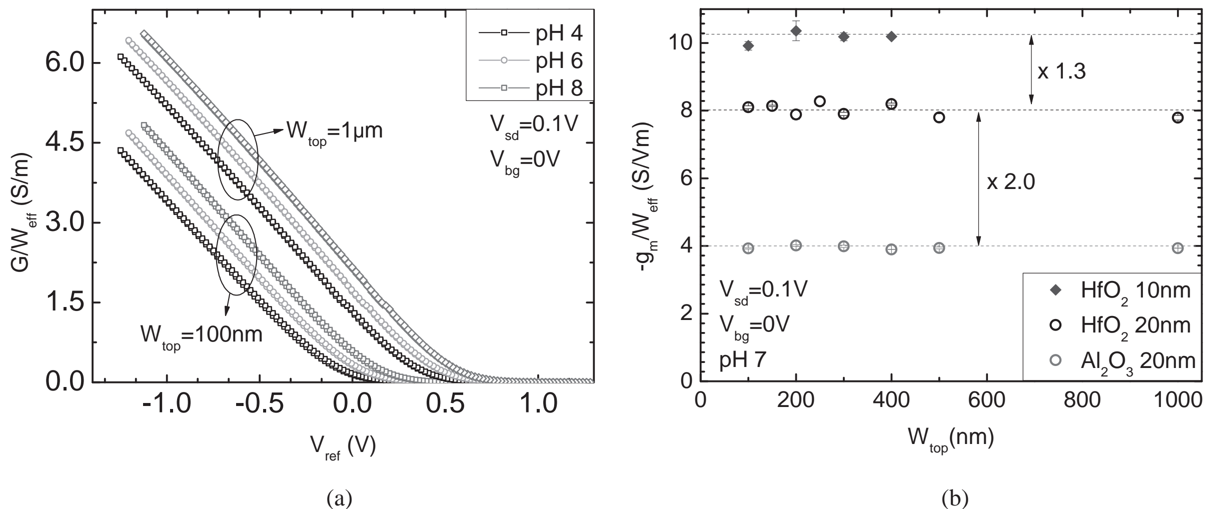

(a) (b)

Fig. 3. (a) Conductance G, normalized with the effective wire width W_{eff} vs the reference voltage V_{ref} for two NWs (W_{top} = 100 nm and 1 μm) measured at pHs 4, 6, and 8. (b) Scaled transconductance g_m/W_{eff}, extracted from the normalized conductance in Fig. 3(a) for different NW widths and gate oxides. It is constant for NW with W_{top} between 100 nm and 1 μm. The dashed line is the calculated average value. The transconductance changes with the oxide type and thickness.

Although the scaled transconductance values are constant for wires of different widths, we have to understand the different g_m/W_{eff} values for different top gate oxides. In the linear regime, g_m is determined by the mobility μ of the charge carriers and the liquid gate capacitance per unit area, C_{lg}:

$$g_m = \mu C_{lg} W_{eff}/L. \quad (2)$$

Here, L denotes the length of the NWs, which was constant for all the wires. We assume that for one sample, the mobility is constant for all the wires of different widths as it is indicated by the constant value of the scaled transconductance. Sample-to-sample variations in the mobility may still occur in the fabrication process. Therefore, the scaling of g_m with W_{eff} will then equally be reflected in the capacitance. As a consequence, the value of the scaled transconductance g_m/W_{eff} should be determined using C_{lg}. The liquid gate voltage is applied to the NW through the liquid via the top oxide (TOX). It, therefore, involves the double-layer C_{dl} in the electrolyte and the top-oxide capacitance C_{TOX} connected in series. Owing to the high ion concentration in the electrolyte of 100 mM, we have $C_{dl} >> C_{TOX}$. In the series connection, this leads to $C_{lg} \approx C_{TOX}$ and

$$g_m/W_{eff} = \mu C_{TOX}/L. \quad (3)$$

Looking at Fig. 3(b), one would naively expect a factor of two difference in the measured g_m/W_{eff} values between the HfO_2 samples with 10 and 20 nm thicknesses, instead of 1.3. To resolve this discrepancy, we determined the dielectric constants ε_r by capacitance-voltage (*C-V*) spectroscopy. We obtained ε_r = 12 and 17 for HfO_2 layers with 10 and 20 nm thicknesses, respectively. The 20-nm-thick Al_2O_3 layer had a dielectric constant ε_r = 7.2. Our results are comparable to the reported values of ε_r = 10 –18[26] and ε_r = 4–10[21] for HfO_2 and Al_2O_3, respectively. From our *C-V* measurements, we see that the dielectric constants are thickness dependent as suggested by the g_m values of the HfO_2 data in Fig. 3(b). The reason for this might be the presence of an interfacial SiO_2 layer of 2 nm maximum thickness, which grows during the ALD process[20] between the Si substrate and the ALD oxides. It reduces the dielectric constant of the total layer, according to the series capacitance of the SiO_2 and the ALD oxide layer. Knowing the dielectric constants of HfO_2 layers, we estimated a C_{TOX} capacitance ratio of 1.4 between the 10- and 20-nm-thick HfO_2 samples. Indeed, this result shows that we cannot expect a factor of two difference in the measured g_m/W_{eff} values in Fig. 3(b). The slight discrepancy between the C_{TOX} capacitance ratio, which is 1.4, and the ratio of 1.3 for g_m/W_{eff} can be attributed to slight differences in the mobility. On the basis of our data, we estimated mobilities of 58 and 62 cm^2/Vs for the 10- and 20-nm-thick HfO_2 samples, respectively. For the Al_2O_3 sample, we obtained an estimated hole mobility of 75 cm^2/Vs. The mobility values are in good agreement with the reported hole mobilities for SOI wafers in the accumulation mode (50–139 cm^2/Vs),[11] with similar doping concentrations. The slightly reduced mobility observed in both samples covered with HfO_2 is in agreement with previous results in the literature, which report a mobility degradation in MOSFETs fabricated with high-κ materials.[27]

4. Conclusions

In conclusion, we have systematically studied the effect of the NW width W_{top} ranging from 100 nm to 1 μm on the pH response of SiNW-ISFET. Here, the pH response is determined from the voltage shift ΔV_{ref} of the transfer curve in mV/pH. SiNW-ISFETs with Al_2O_3 or HfO_2 exhibit an ideal linear Nernstian response of 60 mV/pH at 300 K in the subthreshold and linear regimes, without degradation of the Nernstian pH response over time. The drift rate of V_{ref} is a few mV/h. For future experiments, we suggest to correct and thereby minimize the influence of drift on the sensor response by differential measurements, where a passivated NW is used as the reference NW.(28) No effect of the NW width on the pH response was observed. The results of our systematic study are in strong contrast to those described in previous publications as no effect of the wire width or the operating regime on the pH response is observed. Not only the sensing properties but also the electrical properties of the NWs are exceptionally good and reproducible, *e.g.*, the 48 NWs integrated on one sample have a variation in V_{th} of ~50 mV from NW to NW of the same width. Also, the negligible hysteresis in the transfer curves and leakage currents below 2 nA are the result of our reliable fabrication technique. The hole mobilities and dielectric constants of the ALD oxides are in good agreement with expected values from the literature. We also have proposed a scaling method of the wire conductance using the full top perimeter width in liquid gating experiments, which leads to a constant scaled transconductance for all the wires. The excellent sensing and electrical properties of wires in the 100 nm range prove the feasibility of a dense integration of SiNW arrays, which is demanded for future systems with multiplexing functionality. For multiplexed detection, we suggest differential measurements with a passivated NW as reference wire, in order to minimize disturbances of the signal, such as drift, temperature or nonspecific adsorption.

Acknowledgement

This work was supported by the Swiss federal program Nano-Tera, the Swiss National Science Foundation (SNSF), the Swiss Nanoscience Institute (SNI), and the European Commission under the FP7-NMP project Hysens (263091).

References

1 P. Bergveld: IEEE Trans. Biomed. Eng. **BME-17** (1970) 70.
2 P. Bergveld: Sens. Actuators, B **88** (2003) 1.
3 Y. Cui, Q. Q. Wei, H. K. Park and C. M. Lieber: Science **293** (2001) 1289.
4 X. T. Vu, J. F. Eschermann, R. Stockmann, R. GhoshMoulick, A. Offenhäusser and S. Ingebrandt: Phys. Status Solidi A **206** (2009) 426.
5 S. Chen, J. G. Bomer, E. T. Carlen and A. van den Berg: Nano Lett. **11** (2011) 2334.
6 S. Zafar, C. D'Emic, A. Afzali, B. Fletcher, Y. Zhu and T. Ning: Nanotechnology **22** (2011) 405501.
7 Y. Cui, Z. Zhong, D. Wang, W. U. Wang and C. M. Lieber: Nano Lett. **3** (2003) 149.
8 Y. Cui and C. M. Lieber: Science **291** (2001) 851.

9 G. F. Zheng, F. Patolsky, Y. Cui, W. U. Wang and C. M. Lieber: Nat. Biotechnol. **23** (2005) 1294.
10 B. Tian, T. Cohen-Karni, Q. Qing, X. Duan, P. Xie and C. M. Lieber: Science **329** (2010) 830.
11 E. Stern, J. F. Klemic, D. A. Routenberg, P. N. Wyrembak, D. B. Turner-Evans, A. D. Hamilton, D. A. LaVan, T. M. Fahmy and M. A. Reed: Nature **445** (2007) 519.
12 N. Elfström, R. Juhasz, I. Sychugov, T. Engfeldt, A. E. Karlstrom and J. Linnros: Nano Lett. **7** (2007) 2608.
13 J. H. Ahn, S. J. Choi, J. W. Han, T. J. Park, S. Y. Lee and Y. K. Choi: IEEE Trans. Nanotechnol. **10** (2011) 1405.
14 N. Elfström and J. Linnros: Proc. 17th Int. Vacuum Congress/13th Int. Conf. on Surface Science/Int. Conf. on Nanoscience and Technology, Vol. 100 (J. Phys. Conf. Ser., Bristol, 2008).
15 N. Elfström, A. E. Karlström and J. Linnros: Nano Lett. **8** (2008) 945.
16 X. P. A. Gao, G. Zheng and C. M. Lieber: Nano Lett. **10** (2010) 547.
17 O. Knopfmacher, A. Tarasov, W. Fu, M. Wipf, B. Niesen, M. Calame and C. Schönenberger: Nano Lett. **10** (2010) 2268.
18 O. Knopfmacher, A. Tarasov, M. Wipf, W. Fu, M. Calame and C. Schönenberger: ChemPhysChem **13** (2012) 1157.
19 G. S. May and S. M. Sze: Fundamentals of Semiconductor Fabrication (Wiley, New York, 2007) 1st ed.
20 H. Kim, P. C. McIntyre and K. C. Saraswat: Appl. Phys. Lett. **82** (2003) 106.
21 L. Zhang, H. C. Jiang, C. Liu, J. W. Dong and P. Chow: J. Phys. D: Appl. Phys. **40** (2007) 3707.
22 A. Tarasov, W. Fu, O. Knopfmacher, J. Brunner, M. Calame and C. Schönenberger: Appl. Phys. Lett. **98** (2011) 012114.
23 J. P. Colinge: Silicon-on-Insulator Technology (Springer, Berlin, 2004) 3rd ed.
24 S. M. Koo, Q. L. Li, M. D. Edelstein, C. A. Richter and E. M. Vogel: Nano Lett. **5** (2005) 2519.
25 J. Goldberger, A. I. Hochbaum, R. Fan and P. Yang: Nano Lett. **6** (2006) 973.
26 J. F. Conley, Y. Ono, R. Solanki, G. Stecker and W. Zhuang: Appl. Phys. Lett. **82** (2003) 3508.
27 J. R. Watling, L. F. Yang, A. Asenov, J. R. Barker and S. Roy: IEEE Trans. Device Mater. Reliab. **5** (2005) 103.
28 A. Tarasov, M. Wipf, K. Bedner, J. Kurz, W. Fu, V. A. Guzenko, O. Knopfmacher, R. L. Stoop, M. Calame and C. Schönenberger: Langmuir **28** (2012) 9899.